LBL-27882
Preprint

# Lawrence Berkeley Laboratory
UNIVERSITY OF CALIFORNIA

## Materials & Chemical Sciences Division

Submitted to AIChE Journal

# Mass Transfer in a Small Aspect Ratio Rotating Disk CVD Reactor

D.T. Schwartz and R.H. Muller

September 1989

LOAN COPY
Circulates
for 2 weeks
LBL-27882
Copy 2
Bldg. 50 Library.

Prepared for the U.S. Department of Energy under Contract Number DE-AC03-76SF00098.

## DISCLAIMER

This document was prepared as an account of work sponsored by the United States Government. While this document is believed to contain correct information, neither the United States Government nor any agency thereof, nor the Regents of the University of California, nor any of their employees, makes any warranty, express or implied, or assumes any legal responsibility for the accuracy, completeness, or usefulness of any information, apparatus, product, or process disclosed, or represents that its use would not infringe privately owned rights. Reference herein to any specific commercial product, process, or service by its trade name, trademark, manufacturer, or otherwise, does not necessarily constitute or imply its endorsement, recommendation, or favoring by the United States Government or any agency thereof, or the Regents of the University of California. The views and opinions of authors expressed herein do not necessarily state or reflect those of the United States Government or any agency thereof or the Regents of the University of California.

# Mass Transfer in a Small Aspect Ratio Rotating Disk CVD Reactor

Daniel T. Schwartz* and Rolf H. Muller
Materials and Chemical Sciences Division
Lawrence Berkeley Laboratory
University of California
Berkeley, CA 94720

**Abstract**

The effects of reactant injection velocity, substrate rotation, and fluid properties on thin film deposition in a small aspect ratio rotating disk chemical vapor deposition (CVD) reactor are analyzed by solving the Navier-Stokes and species continuity equations using perturbation techniques. The analysis applies to deposition of a mass-transfer-limited species in the core region of the reactor, where edge effects are negligible. Explicit analytical solutions for the deposition rate at the reactive substrate are found in the limiting cases of large and small Peclet numbers (Pe). A thin concentration boundary layer with characteristics that depend on the Reynolds (Re) and Schmidt (Sc) numbers forms on the rotating disk substrate when Pe is large. The deposition rate for large Pe is shown to be $\sim O(Pe^{1/3})$ when $Re \ll 1$, $\sim O(Pe^{1/2})$ when $Re \gg 1$ and $Sc \ll 1$, and $\sim O(Re^{1/2}Sc^{1/3})$ when $Re \gg 1$ and $Sc \gg 1$. Two-term Sherwood number expansions are shown to agree with exact numerical results to within 10% for the range of Sc, Re, and Rossby numbers employed in CVD. Applications of these analytical results to develop guidelines for the operation of rotating disk CVD reactors are discussed.

* Author to whom correspondence should be addressed.

## Introduction

The growth of thin film materials for electronic device applications requires a high degree of composition and thickness uniformity over large areas. Chemical vapor deposition (CVD) is a common technique employed to form thin layers that satisfy uniformity requirements, but deposition in these systems is generally limited by the rate of reactant mass transfer to the substrate surface (Thompson et al., 1989; Tompa et al., 1989). The deposition of a mass-transfer-limited species is spatially uniform when the concentration boundary layer induced by the reactive substrate is independent of the transverse coordinates. Hence, a major design goal for CVD reactors is to develop configurations that have uniform mass transfer accessibility, i.e. a spatially flat concentration boundary layer (Houtman et al., 1986; Patnaik et al, 1989).

Modern CVD reactor designs are often based on axisymmetric rotating flows where a substrate disk spins with angular velocity $\Omega$ and a reactant stream is injected axially towards the substrate with a uniform velocity V (Wang et al., 1986). This reactor configuration is sometimes called a stagnation point flow reactor when $\Omega=0$ (Houtman et al, 1986), a rotating disk metalorganic CVD reactor (Thompson et al., 1989; Tompa et al., 1989), or an organometalic vapor phase epitaxy reactor (Wang et al., 1986; Patnaik et al., 1989), but here we simply refer to this as a rotating disk reactor (RDR) or a small aspect ratio rotating disk reactor (SARDR), when the reactor aspect ratio (=L/R, see Fig. 1) is less than one.

In the absence of edge effects (i.e. self-similar flow), the SARDR has a planar concentration boundary layer that extends over the entire reactive substrate, even when large axial thermal gradients exist (Evans and Greif, 1988). Convective transport in a SARDR can be considerably more complex than the self-similar case when edge and buoyancy effects are taken into account (Houtman et al., 1986; Evans and Greif, 1987; Patnaik et al., 1989). But, flow visualization (Wang et al., 1986) and numerical studies

(Houtman et al., 1986; Evans and Greif, 1987) have established operating conditions where the RDR response is, for all practical purposes, indistinguishable from the simple one-dimensional, self-similar system. The study of Houtman et al. (1986) is particularly relevant here, since they demonstrated that reducing the reactor aspect ratio from 0.9 to 0.2 displaced edge effects to all but a small region near the perimeter of the reactor. Moreover, both Houtman et al. (1986) and Evans and Greif (1987) have shown that even when the reactor aspect ratio was O(1), a self-similar core region remained in the reactor when forced flow dominated natural convection. The presence of a self-similar core region in a SARDR with edges is fortuitous since, in general, this is not assured for confined axisymmetric rotating flows (Brady and Durlofsky, 1987).

In the self-similar core region of a SARDR (or as the reactor aspect ratio approaches zero) mass transfer is characterized by convective transport between an infinite rotating substrate disk with an infinite coaxial porous injector. This configuration is shown schematically in Fig. 1.

Only limited studies are reported in the literature for heat and mass transfer in the self-similar SARDR configuration. Gorla (1984) has numerically analyzed heat transfer in the related problem of an infinite porous slider bearing with a constant property Newtonian fluid impinging on a translating plane. His numerical results were limited to four Prandtl numbers (Pr) in the range $0.7 \leq Pr \leq 10$ and select Reynolds numbers (Re) in the range $0.01 \leq Re \leq 50$. Evans and Greif (1988) have recently presented a thorough numerical analysis of self-similar flow and heat transfer in the SARDR when helium is the injected fluid. Their study included the effects of disk rotation, fluid injection, and temperature dependent physical properties. They found that large temperature differences between the porous injection disk and the rotating disk can significantly modify heat transfer in the system due to the axial variation of physical properties. Unfortunately, the results presented by Evans and Greif were restricted to the injection of helium gas, since those were the physical properties used in the model. They also considered temperature

independent properties for a fluid with a Prandtl number of Pr=0.67. To the best of our knowledge, no analytical solutions to the problem of convective heat or mass transfer in a SARDR are currently available in the literature.

In this paper we present perturbation expansions for the concentration field and deposition rate induced by a mass-transfer-limited reaction on the rotating disk of a self-similar SARDR. Since a SARDR is often operated with many different injection fluids and temperatures, we derive expressions valid over a wide range of Schmidt numbers (analogous to Pr in heat transfer), Reynolds numbers, and Rossby numbers (a measure of axial flow to rotational flow strength). In the first part of the Results section, perturbation solutions are presented for flow in the SARDR. The velocity field expansions are then applied to the convective-diffusion equation to derive perturbation expansions for the concentration field and Sherwood number (a dimensionless mass transfer coefficient that is analogous to the Nusselt number) at the rotating disk. The Discussion section is devoted to a comparison of our perturbation solutions with numerical solutions available in the literature (Wang, 1974; Gorla, 1984; Evans and Greif, 1988). Our results for the Sherwood number are found to match numerical results to within 5% over the entire range of Schmidt and Reynolds numbers computed by Gorla (1984). The perturbation solutions are also compared with Evans and Greif's numerical results as a function of the inverse Rossby number ($\alpha$), and agreement to within 5% is found when $0 \leq \alpha \leq 10$. For $\alpha > 10$, the Sherwood number at the rotating disk is given to within 8% by the mass transfer rate to a disk rotating in an infinite medium. From these comparisons, we show that the overlap of perturbation expansions with different domains of validity provide good estimates of the Sherwood number at the rotating disk of a SARDR for any value of Re and Sc.

## Problem Formulation

### *Flow field*

Two coaxial disks of infinite extent are taken to form the boundaries of the SARDR. Heterogeneous reaction occurs at the reactive substrate disk ($z = 0$) and reactant fluid is injected from the porous injection disk ($z = L$), see Fig. 1. The bottom disk rotates with an angular velocity of $\Omega$. The injected fluid is assumed to be incompressible (Mach number << 1), Newtonian, and to have constant physical properties (kinematic viscosity $\nu$ and density $\rho$). In addition, the injected fluid is assumed to contain the reactant as a minor component in an inert carrier fluid, as is commonly found in CVD (Thompson et al., 1989); volume changes due to reaction stoichiometry are therefore neglected. Total mass continuity requires that axisymmetric flow confined between the boundaries of the SARDR must be self-similar in form, and the velocity field is given by

$$\mathbf{v} = rf(z)\mathbf{e}_r + rg(z)\mathbf{e}_\theta + w(z)\mathbf{e}_z \,, \tag{1}$$

where $f = v_r/r$ is the radial flow function, $g = v_\theta/r$ is the azimuthal flow function, $w = v_z$ is the axial velocity, r is the radial position, and the unit vectors for a cylindrical coordinate system $(r, \theta, z)$ are given by $\mathbf{e}_r$, $\mathbf{e}_\theta$, and $\mathbf{e}_z$. The flow functions f, g, and w are functions of axial position z only. The nondimensionalized radial and azimuthal components of the momentum equation are

$$\frac{d^3W}{d\eta^3} + \mathrm{Re}\left(2W\frac{d^2W}{d\eta^2} - \left(\frac{dW}{d\eta}\right)^2 + \alpha^2G^2 - \frac{1}{2}\frac{1}{\lambda}\frac{\partial P}{\partial \lambda}\right) = 0 \,, \tag{2a}$$

$$\frac{d^2G}{d\eta^2} + 2\,\mathrm{Re}\left(W\frac{dG}{d\eta} - G\frac{dW}{d\eta}\right) = 0 \,, \tag{2b}$$

and the axial component of momentum is

$$\frac{d^2W}{d\eta^2} + Re\left(2W\frac{dW}{d\eta} + \frac{1}{4}\frac{\partial P}{\partial \eta}\right) = 0 . \tag{2c}$$

Note that mass continuity

$$\frac{dW}{d\eta} - F = 0 , \tag{3}$$

was used to derive Eq. 2. The Reynolds number for this system is defined as $Re = VL/\nu$, $\eta = z/L$ is the axial distance, $\lambda = r/L$ is the radial distance, $\alpha = \Omega L/V$ is the inverse of a rotational Rossby number that measures the relative strength of azimuthal (rotational) flow to axial (injection) flow, $P = 2p/\rho V^2$ is dimensionless pressure, $W = -w/2V$, $G = g/\Omega$, and $F = fL/V$. For Eqs. 2a and 2c to be compatible, the pressure field must take the form

$$-P = A\lambda^2 + \Phi(\eta) , \tag{4}$$

where A is the radial pressure coefficient, and $\Phi$ is a function of $\eta$ that is determined from Eq. 2c. The governing equations 2 - 4 are an exact formulation of the Navier-Stokes equations that are decoupled from species continuity by the assumption of negligible volume change upon reaction and composition independent physical properties.

At the surface of the rotating disk ($\eta = 0$) there is no slip or penetration of fluid,

$$W(0) = \frac{dW}{d\eta}(0) = 0 , \tag{5a}$$

$$G(0) = 1 , \tag{5b}$$

while at the upper disk ($\eta = 1$) there is uniform axial injection

$$W(1) = \frac{1}{2} , \tag{6a}$$

and no slip,

$$\frac{dW}{d\eta}(1) = 0\,, \tag{6b}$$

$$G(1) = 0. \tag{6c}$$

It is interesting to note that the equation governing W is third order (see Eq. 2a), but there are four conditions at the boundary that must be satisfied. The additional constraint is used to determine the unknown radial pressure coefficient A.

## *Concentration field*

Steady mass transport of a dilute species in the self-similar SARDR is governed by axial convection and diffusion, i.e.,

$$v_z \frac{dc}{dz} = D \frac{d^2c}{dz^2}\,, \tag{7}$$

where c is the concentration of the reactant species, and D is the (constant) species diffusivity for the dilute reactant. At the substrate disk surface (z = 0) a heterogeneous reaction is consuming the reactant at the mass-transfer-limited rate, so that

$$c = 0\,, \tag{8}$$

and at the injection disk (z = L)

$$c = c_i\,, \tag{9}$$

where the concentration discharged from the porous disk is given by $c_i$.

The nondimensional form of Eq. 7 is

$$-2PeW(\eta)\frac{dC}{d\eta} = \frac{d^2C}{d\eta^2}\,. \tag{10}$$

where $Pe=VL/D=ReSc$ is the Peclet number, $Sc=\upsilon/D$ is the Schmidt number, and $C=c/c_i$ is the dimensionless concentration. The dimensionless boundary condition at $\eta=0$ is

$$C(0) = 0 , \tag{11}$$

and at $\eta=1$, we have

$$C(1) = 1 . \tag{12}$$

The molar flux at the surface of the rotating disk can be written in terms of a mass transfer coefficient h:

$$D \frac{dc}{dz}(0) = h\, c_i . \tag{13}$$

Nondimensionalizing Eq. 13 provides an expression for the Sherwood number, Sh,

$$Sh = \frac{dC}{d\eta}(0) , \tag{14}$$

where $Sh = hL/D$. The Sherwood number is proportional to the deposition rate of a mass-transfer-limited species in CVD (see Eq. 87) and is also equivalent to the Nusselt number in heat transfer.

## Asymptotic Flow Results

In this section, the limiting cases of low and high Reynolds number flow in the self-similar SARDR are considered. Elkouh (1968) has analyzed low Reynolds number injection flows confined between coaxial rotating porous disks. We extend Elkouh's treatment by formally consider flows dominated by rotation, including the limiting case of low Re flows driven solely by the rotating disk (i.e. $\Omega L/V \rightarrow \infty$). By considering separately the limiting cases of rotation-dominated and injection-dominated flows, the restrictions on Re and $\alpha$ necessary to balance inertial terms in the radial momentum equation are clarified. The equations analyzed here (Eqs. 2 - 6) are therefore nondimensionalized in a manner

somewhat different from those solved by Elkouh. The high Reynolds number self-similar flow of injected and rotating fluid confined between coaxial rotating disks has been analyzed in detail by Wang and Watson (1979). Since the flow field plays an important role in our derivation of convective mass transfer in the SARDR, we include here a brief accounting of known asymptotic results for the hydrodynamics. Most of the steps in the derivation of the perturbation solutions are excluded and the interested reader is referred to Elkouh (1968) and Wang and Watson (1979) for details on the solution methodology for Re<<1 and Re>>1 flows, respectively.

## *Low Reynolds number flow*

When $\alpha^2 << 1$ injection flow dominates rotational flow, and solutions for Eqs. 2 - 6 are found using the straightforward expansions

$$W = W_0 + \mathrm{Re}\, W_1 + O(\mathrm{Re}^2) \ , \tag{15a}$$

$$G = G_0 + \mathrm{Re}\, G_1 + O(\mathrm{Re}^2) \ , \tag{15b}$$

and

$$A = \mathrm{Re}^{-1} A_0 + A_1 + O(\mathrm{Re}) \ . \tag{15c}$$

Equations 15a-c are inserted into Eqs. 2 - 6 and terms of comparable order as Re→0 are solved, yielding

$$W_0 = \frac{3}{2}\eta^2 - \eta^3 , \tag{16a}$$

$$G_0 = 1 - \eta , \tag{16b}$$

$$A_0 = 6 , \tag{16c}$$

$$W_1 = \left(\frac{13}{140}+\frac{\alpha^2}{20}\right)\eta^2 - \left(\frac{9}{70}+\frac{7\alpha^2}{60}\right)\eta^3 + \frac{\alpha^2}{12}\eta^4 - \frac{\alpha^2}{60}\eta^5 + \frac{1}{20}\eta^6 - \frac{1}{70}\eta^7 , \tag{17a}$$

$$G_1 = -\frac{9}{20}\eta + \eta^3 - \frac{3}{4}\eta^4 + \frac{1}{5}\eta^5 , \tag{17b}$$

and

$$A_1 = \frac{27}{35} - \frac{3\alpha^2}{10} . \tag{17c}$$

It is interesting to note that the azimuthal flow function G is independent of $\alpha$ (to the order calculated), but the axial flow W does depend on $\alpha$. As $\alpha^2 \rightarrow 0$ the axial flow takes on the form of a pure injection flow with no contribution from centrifugal forces.

When rotational flow dominates over injection flow (i.e. $\alpha^2 >> 1$), it is worthwhile rescaling the governing equations to balance the inertial terms in Eq. 2a. A new set of dimensionless variables are defined in the following manner: $W = \alpha\overline{W}$, $G = \overline{G}$, $A = \alpha^2\overline{A}$, $\overline{Re} = \alpha Re = \Omega L^2/\nu$, where we note that the Reynolds number is now based on the rotational velocity of the disk. Substituting these variables into Eqs. 2a and 2b provides the rescaled radial and azimuthal momentum equations

$$\frac{d^3\overline{W}}{d\eta^3} + \overline{Re}\left(2\overline{W}\frac{d^2\overline{W}}{d\eta^2} - \left(\frac{d\overline{W}}{d\eta}\right)^2 + \overline{G}^2 + \overline{A}\right) = 0 \tag{18a}$$

and

$$\frac{d^2\overline{G}}{d\eta^2} + 2\,\overline{Re}\left(\overline{W}\frac{d\overline{G}}{d\eta} - \overline{G}\frac{d\overline{W}}{d\eta}\right) = 0 . \tag{18b}$$

The boundary conditions are

$$\overline{W} = \frac{d\overline{W}}{d\eta} = 0 , \ \overline{G} = 1 \quad \text{at } \eta = 0 , \tag{19a,b,c}$$

and

$$\frac{d\overline{W}}{d\eta} = 0 , \ \overline{W} = \frac{1}{2\alpha} , \ \overline{G} = 0 \quad \text{at } \eta = 1 . \tag{20a,b,c}$$

Straightforward expansions analogous to Eqs. 15a-c are written for $\overline{W}$, $\overline{G}$, and $\overline{A}$ in terms of a series in $\overline{Re}$ ,

$$\overline{W} = \overline{W}_0 + \overline{Re}\,\overline{W}_1 + O(\overline{Re}^2) , \tag{21a}$$

$$\overline{G} = \overline{G}_0 + \overline{Re}\,\overline{G}_1 + O(\overline{Re}^2) , \tag{21b}$$

and

$$\overline{A} = \overline{Re}^{-1}\,\overline{A}_0 + \overline{A}_1 + O(\overline{Re}) . \tag{21c}$$

Collecting terms of comparable order as $\overline{Re}\rightarrow 0$ and solving for $\overline{W}_n$, $\overline{G}_n$, and $\overline{A}_n$ gives

$$\overline{W}_0 = \frac{3}{2\alpha}\eta^2 - \frac{1}{\alpha}\eta^3 , \tag{22a}$$

$$\overline{G}_0 = 1 - \eta , \tag{22b}$$

$$\overline{A}_0 = \frac{6}{\alpha}, \tag{22c}$$

$$\overline{W}_1 = \left(\frac{13}{140\alpha^2} + \frac{1}{20}\right)\eta^2 - \left(\frac{9}{70\alpha^2} + \frac{7}{60}\right)\eta^3 + \frac{1}{12}\eta^4 - \frac{1}{60}\eta^5 + \frac{1}{20\alpha^2}\eta^6 - \frac{1}{70\alpha^2}\eta^7, \tag{23a}$$

$$\overline{G}_1 = -\frac{9}{20\alpha}\eta + \frac{1}{\alpha}\eta^3 - \frac{3}{4\alpha}\eta^4 + \frac{1}{5\alpha}\eta^5 , \tag{23b}$$

and

$$\overline{A}_1 = \frac{27}{35\alpha^2} - \frac{3}{10} . \tag{23c}$$

In the limit of $\alpha^2\rightarrow\infty$, the flow field, represented by Eqs. 21 - 23, takes the low Reynolds number form of a purely rotational flow confined between a rotating disk and a stationary disk (Lance and Rogers, 1962). The formal difference between the large and small $\alpha$

expansions (Eqs. 15 and 21) is that a constraint on the product $\alpha$Re (i.e. $\overline{\mathrm{Re}}<<1$) must be satisfied by Eq. 21, whereas Eq. 15 need only satisfy the constraint Re<<1.

Note that the perturbation solution scaled for $\alpha^2>>1$ (Eqs. 21-23) are identical to the solution scaled for $\alpha^2<<1$ (Eqs. 15-17) when $\alpha = 1$. It is plain that the solutions for $\alpha^2>>1$ and $\alpha^2<<1$ overlap in the intermediate range of $\alpha^2 \sim O(1)$, since the criteria used in formulating Eqs. 15 and 21, Re<<1 and $\overline{\mathrm{Re}}<<1$, respectively, are both satisfied simultaneously. In fact, either set of expansions (Eqs. 15 or 21) hold for small Reynolds numbers, provided that all of the inertial terms are small, including centrifugal forces. In other words, for any finite $\alpha$ there exists a value of Re sufficiently small for all inertial terms in the radial momentum equation 2a to be negligible at leading order; rescaling Eqs. 15 (to get Eqs. 21) simply illuminates the conditions where the inertial terms are balanced for large $\alpha$.

## *High Reynolds number flow with finite $\alpha$*

High Reynolds number axisymmetric rotating flows with no injection of fluid have been intensely studied owing to their self-similar form, the multiplicity of possible steady state solutions (Zandbergen and Dijkstra, 1987), and the sensitivity of flow to edge effects (Brady and Durlofsky, 1987). Injection-dominated high Reynolds number axisymmetric flows seem to be less complex in their structure (Wang, 1974; Wang and Watson, 1979). We first consider the case of pure injection with no rotation ($\alpha$=0), and then modifications to the far-field equations are presented to account for the rotating substrate disk.

When $\alpha$=0 the radial momentum equation 2a is decoupled from Eq. 2b. Differentiating Eq. 2a with respect to $\eta$ yields the fourth order differential equation

$$\frac{1}{\mathrm{Re}}\frac{d^4W}{d\eta^4} + 2W\frac{d^3W}{d\eta^3} = 0\,. \tag{24}$$

At the substrate disk surface, Eqs. 5a hold, and at the upper disk Eqs. 6a and 6b must be satisfied. Mass continuity, Eq. 3, provides an equation for determining the radial flow function F, and the radial pressure gradient is determined from Eqs. 2a and 4, once W is known. Equation 24 becomes singular when $Re \rightarrow \infty$, indicating that a boundary layer forms near the bottom disk. The governing equation 24 and its boundary conditions are identical to the equations for boundary layer flow beneath a circular porous slider bearing (Wang, 1974). In his studies of slider bearings, Wang found that the thickness of the viscous boundary layer that forms near the plane $\eta=0$ scaled as $O(Re^{-1/2})$, when $Re \rightarrow \infty$. This scaling gave rise to an inner solution series of the form

$$W(\eta) = Re^{-1/2} W_0 + Re^{-1} W_1 + O(Re^{-3/2}) \ . \tag{25}$$

The uniformly valid large Reynolds number two-term composite solution to Eq. 24 is (Wang, 1974)

$$W = -\frac{1}{2}\eta^2 + Re^{-1/2}[-m(\eta^2 - 2\eta) + \varphi(\xi)] + O(Re^{-1}) , \tag{26}$$

where $\xi = \sqrt{Re}\,\eta$ is the stretched inner variable for the boundary layer region, m=0.56894 is a constant found in matching the inner and outer solutions, and $\varphi(\xi)$ is the classic solution for axisymmetric stagnation point flow against a stationary flat plate (Homann, 1936). The function $\varphi(\xi)$ was derived by Homann as a series solution

$$\varphi(\xi) = a_0 + a_1\xi^1 + a_2\xi^2 + a_3\xi^3 + a_4\xi^4 + a_5\xi^5 + \ldots \tag{27}$$

where $a_i$ are constants. The first twenty five terms of Eq. 27 were tabulated originally by Homann; the coefficients $a_0$ and $a_1$ are identically zero.

When the bottom disk rotates, the composite solution series for W resembles Eq. 26, except that numerical techniques must be used to determine the rotating boundary layer contribution to the composite expansion (Wang and Watson, 1979). In the outer region of the boundary layer, the flow field is modified by the presence of the rotating disk; this is seen by comparing the far-field behavior of the inner expansion for the two cases of no

rotation and finite rotation of the substrate. When $\alpha$=0, Homann's function $\varphi(\xi)$ has the limiting form

$$\lim_{\xi\to\infty} \varphi(\xi) = \xi - m \tag{28}$$

where m is the constant given following Eq. 26. Recall that $\xi$ is the stretched inner variable. Wang and Watson (1979) have shown that the far-field function, Eq. 28, can be generalized when the bottom disk rotates and the injection disk is stationary, i.e.,

$$\lim_{\xi\to\infty} \varphi(\xi) = \xi - M(\alpha)\,, \tag{29}$$

where $M(\alpha)$ now depends on the value of $\alpha$. Thus, Eq. 29 changes the matching criteria between the inner and outer solutions when the substrate rotates. The function $M(\alpha)$ has been determined numerically by Wang and Watson for $\alpha = 0$, 5, and 10. In this range of $\alpha$, $M(\alpha)$ is nearly linear, and the function is given approximately by

$$M(\alpha) = 0.56894 - 0.1105\,\alpha\,, \tag{30}$$

for $0\le\alpha\le10$. M(0) is identical to the constant m. The two-term expansion for the axial component of flow is found by inserting Eq. 29 into Eq. 26 and replacing m with $M(\alpha)$:

$$W = \eta - \frac{1}{2}\eta^2 + Re^{-1/2}\,[\,-M(\alpha)\,(\eta - 1)^2] + O(Re^{-1})\,, \tag{31}$$

where $M(\alpha)$ is given approximately by Eq. 30. It is important to recognize that Eq. 31 breaks down when $\xi\,[\equiv\sqrt{Re}\,\eta\,] \sim O(1)$ (or smaller) since the function $\varphi(\xi)$ given by Eq. 29 is not valid for that region of the inner layer.

## *High Reynolds number rotational flow ($\alpha\to\infty$)*

It was noted in the preceding section that the stability and structure of high Reynolds number flows dominated by rotation is complex. One of the high Reynolds number solution branches found by Mellor, Chapple, and Stokes (1968) for self-similar flow with no injection from the porous disk (i.e. $\overline{Re}\to\infty$ and $\alpha^2\to\infty$) takes the form of a von Kàrmàn flow induced by a rotating disk in an infinite quiescent medium. Brady and Durlofsky (1987) also found a high Reynolds number ($\overline{Re}$>250) solution branch that

resembled von Kàrmàn rotating disk flow when finite disks with open edges were analyzed. Many CVD reactor models have assumed that von Kàrmàn free-disk flow was applicable in their derivation of convective mass transport. Nonetheless, flow and mass transfer with large $\overline{Re}$ and large $\alpha$ is not analyzed in detail here. Rather, we consider briefly in the Discussion section the limiting behavior of free-disk mass transfer and compare that with Evans and Greif's (1988) numerical solutions. Readers interested in free-disk mass transfer in CVD reactors are referred to Olander (1967), Pollard and Newman (1980), and Hitchman and Curtis (1982) for additional information.

## Mass Transfer in the SARDR

Reactant species are transported to the substrate surface $\eta=0$ by convection and diffusion, see Eq. 10. The importance of convective transport relative to diffusive transport is characterized by the Peclet number ($Pe = VL/D$) for the system. For $Pe>>1$, convection is the dominant mode of mass transfer, except for a region very near the reactive substrate surface. Conversely, for $Pe<<1$, diffusion is the dominant mode of mass transfer.

A general solution to the convective-diffusion equation 10 and its boundary conditions, Eqs. 11 and 12, is

$$C(\eta) = \frac{\displaystyle\int_0^{\eta} \exp\left(-2Pe\int_0^{\gamma} W(\tau)\,d\tau\right)d\gamma}{\displaystyle\int_0^{1} \exp\left(-2Pe\int_0^{\gamma} W(\tau)\,d\tau\right)d\gamma}, \tag{32}$$

where $\tau$ and $\gamma$ are dummy variables of integration. Numerical methods must be used in general to solve these integrals. Explicit solution to the integrals in Eq. 32 can be found for certain simple forms of the axial velocity W, but not with the axial velocities presented in the preceding section. Perturbation techniques offer an alternative to solving Eq. 32. Using

perturbation analysis, limiting cases of large and small Peclet numbers can be solved explicitly. These limiting cases are analyzed in the following sections.

## Small Peclet Number Mass Transfer (Pe<<1)

As noted above, small Peclet number mass transfer is dominated by diffusive transport. Nevertheless, convection modifies the pure diffusion (Pe→0) limit. The concentration field is expressed as the regular perturbation series

$$C(\eta) = C_0 + Pe\, C_1 + O(Pe^2) . \tag{33}$$

Substituting Eq. 33 into Eqs. 10 - 12, and collecting terms of comparable order as Pe→0 provides the governing equations and boundary conditions for $C_o$, $C_1$, and higher order functions. The zeroth-order equation is

$$\frac{d^2C_o}{d\eta^2} = 0 , \tag{34}$$

with the boundary conditions

$$C_o(0) = 0 \tag{35}$$

and

$$C_o(1) = 1 . \tag{36}$$

The solution to Eqs. 34 - 36 is

$$C_o = \eta . \tag{37}$$

The first-order equation includes the effects of convection and is given by

$$-2W(\eta)\frac{dC_o}{d\eta} = \frac{d^2C_1}{d\eta^2} , \tag{38}$$

with the boundary conditions

$$C_1(0) = C_1(1) = 0 \ . \tag{39a,b}$$

Equation 38 is integrated twice to obtain $C_1$, once the dimensionless axial velocity W is specified. The boundary conditions (Eqs. 39a and 39b) are used to specify the constants of integration. In the following three subsections, the limiting forms of W presented earlier are used to derive $C_1$ and the Sherwood number at the reactive disk surface.

### *Pe<<1 mass transfer with Re, $\overline{Re}$<<1*

First we consider the concentration field perturbation $C_1$ introduced by injection dominated ($\alpha \leq 1$) low Reynolds number flow. Substituting Eqs. 15a-17a into Eq. 38, and integrating twice yields the solution for $C_1$:

$$C_1 = K_1 + K_2\eta - \frac{1}{4}\eta^4 + \frac{1}{10}\eta^5 +$$

$$Re\left(\left(-\frac{13}{840} - \frac{\alpha^2}{120}\right)\eta^4 + \left(\frac{9}{700} + \frac{7\alpha^2}{600}\right)\eta^5 - \frac{\alpha^2}{180}\eta^6 + \frac{\alpha^2}{1260}\eta^7 - \frac{1}{560}\eta^8 + \frac{1}{2520}\eta^9\right), \tag{40}$$

where the integration constants, $K_1$=0 and $K_2$=0.15 + Re[0.004008 + 0.001429$\alpha^2$], are determined from Eqs. 39a and 39b.

The quantity of interest for deposition studies is the Sherwood number, Sh, evaluated at the reactive disk $\eta$=0. The Sherwood number is proportional to the deposition rate (see Eq. 87) and is given in our variables by the derivative of C with respect to $\eta$. Differentiating Eq. 33 with respect to $\eta$ and inserting Eqs. 37 and 40, we find

$$Sh = 1 + Pe\left(0.15 + Re[0.004008 + 0.001429\alpha^2]\right) + O(Pe^2) \ , \tag{41}$$

when Pe<<1, Re<<1, and $\alpha \leq 1$.

The effects of rotation-dominated ($\alpha \geq 1$) low Reynolds number flow on small Peclet number mass transfer are calculated next. Recall that the axial velocity was rescaled for flows dominated by rotation. Inserting the rescaled axial velocity, $W=\alpha\overline{W}$, into the

convective-diffusion equation and defining a new Peclet number based on the angular velocity of the disk, $\overline{Pe} = \alpha Pe = \Omega L^2/D$, gives an equation identical to Eq. 10 with $\overline{Pe}$ replacing Pe. A regular perturbation series in powers of $\overline{Pe}$ (analogous to Eq. 33) is inserted into the convective-diffusion equation. The solution to the zeroth-order equation remains Eq. 37. The first-order equation is identical to Eq. 38 with $\overline{W}$ replacing W. The solution to the first-order equation, using $\overline{W}$ given by Eqs. 21a-23a, is

$$C_1 = K_1 + K_2\eta - \frac{1}{4\alpha}\eta^4 + \frac{1}{10\alpha}\eta^5 +$$
$$\overline{Re}\left(\left(-\frac{13}{840\alpha^2} - \frac{1}{120}\right)\eta^4 + \left(\frac{9}{700\alpha^2} + \frac{7}{600}\right)\eta^5 - \frac{1}{180}\eta^6 + \frac{1}{1260}\eta^7 - \frac{1}{560\alpha^2}\eta^8 + \frac{1}{2520\alpha^2}\eta^9\right), \quad (42)$$

where $K_1=0$ and $K_2=0.15/\alpha + \overline{Re}[0.001429 + 0.004008/\alpha^2]$. The Sherwood number at the reactive disk surface is

$$Sh = 1 + \overline{Pe}\left(0.15/\alpha + \overline{Re}[0.001429 + 0.004008/\alpha^2]\right) + O(\overline{Pe}^2) \quad (43)$$

when $\overline{Pe}<<1$, $\overline{Re}<<1$, and $\alpha \geq 1$.

## *Pe<<1 mass transfer with Re>>1*

In this section, we consider the first-order concentration field perturbation in the SARDR system when Pe<<1 and Re>>1. For small Peclet numbers we know that concentration variations occur over the geometric length scale, i.e. O(1), whereas the hydrodynamic boundary layer thickness is $O(Re^{-1/2})$, for large Re. It is appropriate in this case to use the hydrodynamic approximation given by Eq. 31. Substituting Eq. 31 into Eq. 38 and integrating twice yields

$$C_1 = K_1 + K_2\eta - \frac{1}{3}\eta^3 + \frac{1}{12}\eta^4 + 2M(\alpha)Re^{-1/2}\left(\frac{1}{12}\eta^4 - \frac{1}{3}\eta^3 + \frac{1}{2}\eta^2\right), \quad (44)$$

where $K_1=0$ and $K_2=0.25 - 0.5\,M(\alpha)Re^{-1/2}$. The Sherwood number at $\eta=0$ is

$$Sh = 1 + Pe\left(0.25 - 0.5\,M(\alpha)Re^{-1/2}\right) + O(Pe^2) \tag{45}$$

when $Pe<<1$, $Re>>1$, and $\alpha$ finite. $M(\alpha)$ is given by Eq. 30 when $0\leq\alpha\leq10$.

## Large Peclet Number Mass Transfer (Pe>>1)

When $Pe>>1$, concentration gradients are negligible throughout the SARDR, except in the neighborhood of the reactive substrate disk. The nature of the concentration boundary layer that forms near $\eta=0$ depends on the Reynolds number of the flow. When Re is small, the characteristic hydrodynamic length scale is fixed by the geometric length and is O(1). But for large Re, a hydrodynamic boundary layer with thickness $O(Re^{-1/2})$ forms near the bottom disk. Since a hydrodynamic boundary layer and a concentration boundary layer both exists when $Re>>1$ and $Pe>>1$, the solution technique employed depends on whether the concentration boundary layer is confined within, or is external to, the hydrodynamic boundary layer. The effects of the different flow regimes and boundary layer structures on large Peclet number mass transfer are illustrated in the following subsections.

### *Pe>>1 mass transfer with small Reynolds numbers*

Axial flow in the vicinity of the substrate disk can be represented by a Taylor series expansion in terms of $\eta$, i.e.,

$$W = W(0) + W'(0)\eta + \frac{1}{2}W''(0)\eta^2 + \frac{1}{6}W'''(0)\eta^3 + \ldots, \tag{46}$$

where the prime ( ' ) denotes differentiation with respect to $\eta$. An identical expansion can be written for $\overline{W}$. The first two terms on the right hand side of Eq. 46 are identically zero from the boundary conditions (Eqs. 5a). Substituting the first two nonzero terms of Eq. 46

into Eq. 10 provides a governing equation for mass transfer that is accurate near the reactive disk:

$$\frac{1}{Pe}\frac{d^2C}{d\eta^2} + \left(W''(0)\,\eta^2 + \frac{1}{3}W'''(0)\,\eta^3\right)\frac{dC}{d\eta} = 0\,. \tag{47}$$

It is interesting to note that in the case of small Reynolds number flows, $W''(0)$ and $W'''(0)$ [or $\overline{W}''(0)$ and $\overline{W}'''(0)$] are O(1) functions (see Eqs. 81–84). Hence, Eq. 47 can be solved for small Reynolds numbers, subject to the boundary conditions Eqs. 11 and 12, without specifying $W''(0)$ or $W'''(0)$ *a priori.*

Equation 47 is solved using the method of matched asymptotic expansions. A small parameter $\varepsilon$ is defined as

$$\varepsilon = Pe^{-1/3} \tag{48}$$

for Pe>>1. The outer expansion series

$$C^O = C_0^O + \varepsilon C_1^O + O(\varepsilon^2) \tag{49}$$

is substituted for C in Eq. 47 and terms of comparable order in $\varepsilon$ are collected to give

$$\frac{dC_n^O}{d\eta} = 0\,, \tag{50}$$

where n = 0 and 1. Solving Eq. 50 subject to boundary condition Eq. 12 provides the outer expansion solutions $C_0^O = 1$ and $C_1^O = 0$.

We define a stretched variable $\zeta$ in the boundary layer near $\eta$=0,

$$\zeta = \left(\frac{W''(0)}{3}\right)^{1/3}\frac{1}{\varepsilon}\eta\,, \tag{51}$$

and expand C in the inner region as an $\varepsilon$ power series

$$C = C_0^I(\zeta) + \varepsilon C_1^I(\zeta) + O(\varepsilon^2) \ . \tag{52}$$

Substituting Eqs. 48, 51, and 52 into Eq. 47 and equating terms of comparable magnitude as $\varepsilon \to 0$ provides the zeroth-order inner equation

$$\frac{d^2C_0^I}{d\zeta^2} + 3\zeta^2 \frac{dC_0^I}{d\zeta} = 0 \ , \tag{53}$$

the first-order inner equation

$$\frac{d^2C_1^I}{d\zeta^2} + 3\zeta^2 \frac{dC_1^I}{d\zeta} = -W'''(0)\left(\frac{3}{W''(0)^4}\right)^{1/3} \zeta^3 \frac{dC_0^I}{d\zeta} \ , \tag{54}$$

and higher order equations. At the substrate disk surface $\zeta=0$, the boundary conditions are

$$C_0^I(0) = C_1^I(0) = 0 \ , \tag{55}$$

and far from the disk as $\zeta \to \infty$, the boundary conditions matched with the outer solutions are

$$C_0^I(\infty) = 1, C_1^I(\infty) = 0 \ . \tag{56}$$

The solution to the zeroth-order equation 53, subject to the boundary conditions, Eqs. 55 and 56, is

$$C_0^I = \frac{1}{\Gamma\left(\frac{4}{3}\right)} \int_0^\zeta e^{-\gamma^3} d\gamma \ , \tag{57}$$

where $\Gamma(a)$ is the gamma function of a, and $\Gamma(4/3) = 0.89298$. The solution to the first-order equation is found by substituting Eq. 57 into the right hand side of Eq. 54 and

integrating twice. Applying the boundary conditions (Eqs. 55 and 56) to the double integration yields

$$C_1^I = \frac{W'''(0)}{4\Gamma\left(\frac{4}{3}\right)}\left(\frac{3}{W''(0)^4}\right)^{1/3}\int_0^{\zeta} e^{-\gamma^3}\left(\frac{\Gamma\left(\frac{5}{3}\right)}{3\Gamma\left(\frac{4}{3}\right)} - \gamma^4\right)d\gamma \ , \tag{58}$$

where $\Gamma(5/3) = 0.90275$. The composite expansion is identical to the inner solution series.

The Sherwood number at the bottom disk, derived by differentiating Eq. 52 with respect to $\eta$ and inserting the inner solutions, Eqs. 57 and 58, is

$$Sh = \frac{1}{\Gamma\left(\frac{4}{3}\right)}\left(\frac{W''(0)}{3}\right)^{1/3} Pe^{1/3} + \frac{\Gamma\left(\frac{5}{3}\right)}{12\Gamma\left(\frac{4}{3}\right)^2}\frac{W'''(0)}{W''(0)} + O(Pe^{-1/3}) \ . \tag{59}$$

when Pe>>1 and Re<<1. The Sherwood number for rotation-dominated small $\overline{Re}$ is identical to Eq. 59 with $\overline{Pe}$ replacing Pe, $\overline{W}''(0)$ replacing $W''(0)$, and $\overline{W}'''(0)$ replacing $W'''(0)$. The values of $W''(0)$ and $W'''(0)$ are given by Eqs. 81 and 82, respectively, and $\overline{W}''(0)$ and $\overline{W}'''(0)$ are given by Eqs. 83 and 84, respectively.

## *Pe>>1 mass transfer with large Reynolds numbers and finite $\alpha$*

When the Peclet number and the Reynolds number are both large, hydrodynamic and concentration boundary layers form near the substrate disk surface. Two limiting situations may arise when both a hydrodynamic and concentration boundary layer exist; the concentration boundary layer may be much thicker than the hydrodynamic layer, or vice versa. The relative thickness of the hydrodynamic boundary layer to the concentration boundary layer depends on the value of the Schmidt number ($Sc=\upsilon/D$) (Bird et al., 1960).

When Sc<<1, the concentration boundary layer is much thicker than the hydrodynamic boundary layer, while the opposite is true for Sc>>1.

We consider first the case where the Schmidt number is small, Re is large, and their product, the Peclet number, is also large. In this situation, variations in concentration occur over a distance much greater than the hydrodynamic boundary layer thickness $O(Re^{-1/2})$, but much less than the geometric length O(1). When Sc is small, the axial velocity, Eq. 31, is substituted into the convective-diffusion equation to yield

$$\frac{1}{Pe}\frac{d^2C}{d\eta^2} + \left(2\eta - \eta^2 - 2M(\alpha)Re^{-1/2}(\eta - 1)^2\right)\frac{dC}{d\eta} = 0 \ , \tag{60}$$

where $M(\alpha)$ is given by Eq. 30 when $0 \le \alpha \le 10$. Equations 11 and 12, are applied at $\eta = 0$ and $\eta = 1$, respectively. Equation 60 is solved using the method of matched asymptotic expansions. The least degenerate form of Eq. 60 arises when a small parameter $\varepsilon$ is defined by

$$\varepsilon = Pe^{-1/2} . \tag{61}$$

The outer expansion series is identical to Eq. 49, where $\varepsilon$ is now defined by Eq. 61, and the solution to each outer expansion term is $C_0^O = 1$, and $C_n^O = 0$, for all integers $n \ge 1$.

A stretched inner variable $\chi$ is defined in the concentration boundary layer

$$\chi = \frac{1}{\varepsilon}\eta \ , \tag{62}$$

and C is expanded with an $\varepsilon$ power series

$$C = C_0^I(\chi) + \varepsilon C_1^I(\chi) + O(\varepsilon^2) \ . \tag{63}$$

Substituting Eqs. 61, 62, and 63 into Eq. 60 and equating terms of comparable magnitude as $\varepsilon \rightarrow 0$ provides the zeroth-order equation

$$\frac{d^2C_0^I}{d\chi^2} + \left((2 + 4M(\alpha)Re^{-1/2})\,\chi - 2M(\alpha)Sc^{1/2}\right)\frac{dC_0^I}{d\chi} = 0 \ , \tag{64}$$

the first-order equation

$$\frac{d^2C_1^I}{d\chi^2} + \left((2 + 4M(\alpha)Re^{-1/2})\,\chi - 2M(\alpha)Sc^{1/2}\right)\frac{dC_1^I}{d\chi} = \left(1 + 2M(\alpha)Re^{-1/2}\right)\chi^2\frac{dC_0^I}{d\chi}, \tag{65}$$

and higher order equations. At the disk surface $\chi=0$, the boundary conditions are

$$C_0^I(0) = C_1^I(0) = 0 \ , \tag{66}$$

and far from the disk as $\chi \rightarrow \infty$, the boundary conditions matched with the outer solutions are

$$C_0^I(\infty) = 1 \text{ and } C_1^I(\infty) = 0 \, . \tag{67}$$

The solution to the zeroth-order equation 64, subject to the boundary conditions, Eqs. 66 and 67, is

$$C_0^I = \frac{1}{I}\int_0^{\chi} e^{-[(1 + 2M(\alpha)Re^{-1/2})\gamma^2 - 2M(\alpha)Sc^{1/2}\gamma]}\, d\gamma, \tag{68}$$

where

$$I = \int_0^{\infty} e^{-[(1 + 2M(\alpha)Re^{-1/2})\gamma^2 - 2M(\alpha)Sc^{1/2}\gamma]}\, d\gamma \ . \tag{69}$$

The solution to the first-order equation 65 with Eq. 68 substituted into the right hand side, and subject to the boundary conditions, Eqs. 66 and 67, is

$$C_1^I = \int_0^{\chi} \left( \frac{1 + 2M(\alpha)Re^{-1/2}}{3\,I} \gamma^3 + K \right) e^{-[(1 + 2M(\alpha)Re^{-1/2})\gamma^2 - 2M(\alpha)Sc^{1/2}\gamma]}\, d\gamma, \quad (70)$$

where K is an integration constant given by

$$K = - \frac{1 + 2M(\alpha)Re^{-1/2}}{3\,I^2} \int_0^{\infty} \gamma^3\, e^{-[(1 + 2M(\alpha)Re^{-1/2})\gamma^2 - 2M(\alpha)Sc^{1/2}\gamma]}\, d\gamma\ . \quad (71)$$

The composite solution for C is identical to the inner solution series.

Solutions for the integrals I and K are necessary in order to obtain an explicit formulation of the Sherwood number at the rotating disk. The integral I can be approximated by taking advantage of the fact that Sc is small and Re is large. Writing Eq. 69 as the sum of two integrals,

$$I = I_1 + I_2 = \int_0^{Sc^{1/2}} e^{-[(1 + 2M(\alpha)Re^{-1/2})\gamma^2 - 2M(\alpha)Sc^{1/2}\gamma]}\, d\gamma + \int_{Sc^{1/2}}^{\infty} e^{-[(1 + 2M(\alpha)Re^{-1/2})\gamma^2 - 2M(\alpha)Sc^{1/2}\gamma]}\, d\gamma\ , \quad (72)$$

we see that the exponential integrand in $I_1$ can be expanded as a Taylor series since $(1+2MRe^{-1/2})\gamma^2 - 2MSc^{1/2}\gamma << 1$ for small Sc and $\gamma \in [0,Sc^{1/2}]$. The exponential in $I_2$ is approximated with $\exp(-\gamma^2)$, since $\gamma^2 >> (2MRe^{-1/2}\gamma^2 - 2MSc^{1/2}\gamma)$ for small Sc, large Re, and $\gamma$ greater than $Sc^{1/2}$. Given these approximations, the asymptotic solution to $I_1$ for small $Sc^{1/2}$ and large Re is

$$I_1 \sim Sc^{1/2} - \left( \tfrac{1}{3} + [\tfrac{2}{3} Re^{-1/2} - 1]\, M(\alpha) \right) Sc^{3/2}\ , \quad (73a)$$

and the asymptotic solution to integral $I_2$ for small $Sc^{1/2}$ and large Re is

$$I_2 \sim \frac{\sqrt{\pi}}{2} - Sc^{1/2} + \frac{1}{3}Sc^{3/2} . \tag{73b}$$

The integral I is found by summing $I_1$ and $I_2$ :

$$I \sim \frac{\sqrt{\pi}}{2} + [1 - \tfrac{2}{3}Re^{-1/2}]\, M(\alpha)Sc^{3/2} , \tag{74}$$

where Sc is small and Re is large. The integral K, Eq. 71, is broken into two integrals and solved in a manner analogous to Eq. 72, subject to the same approximations. The asymptotic solutions for $K_1$ and $K_2$,

$$K_1 \sim - \frac{1 + 2M(\alpha)Re^{-1/2}}{3\, I^2} \left(\tfrac{1}{4}Sc^2 + [\tfrac{2}{5}M(\alpha) - \tfrac{1}{6} - \tfrac{1}{3}M(\alpha)Re^{-1/2}]Sc^3\right) , \tag{75a}$$

and

$$K_2 \sim - \frac{1 + 2M(\alpha)Re^{-1/2}}{6\, I^2} (1 + Sc)\, e^{-Sc} , \tag{75b}$$

are valid when Sc<<1 and Re>>1 . The sum of $K_1$ and $K_2$ is K. The Sherwood number at the rotating disk is given by

$$Sh = \frac{1}{I} Pe^{1/2} + K + O(Pe^{-1/2}) , \tag{76}$$

when Pe>>1, Re>>1, and Sc<<1.

Note from the zeroth and first-order equations 64 and 65 that in the limit Re→∞ and Sc→0, the large Peclet number concentration field expansion is

$$C(\chi) = \mathrm{erf}(\chi) + \frac{1}{3\sqrt{\pi}} [1 - \mathrm{erf}(\chi) - (1 + \chi^2)\, e^{-\chi^2}]\, Pe^{-1/2} + O(Pe^{-1}) , \tag{77}$$

and the Sherwood number expansion is

$$Sh = \frac{2}{\sqrt{\pi}} Pe^{1/2} - \frac{2}{3\pi} + O(Pe^{-1/2}) . \tag{78}$$

We next consider large Re flow and large Pe mass transfer when the concentration boundary layer is confined within the hydrodynamic boundary layer, i.e. Sc>>1. A solution to the flow field very near the $\eta=0$ substrate disk is necessary in order to determine the Sherwood number. For the case of a rotating disk, an explicit analytical expression for the axial velocity in the hydrodynamic boundary layer is unknown, but when the bottom disk is stationary the axial velocity is given by Eq. 26. Here we consider convective mass transfer in the limit of invicid $Re \rightarrow \infty$ flow with no rotation at the bottom disk ($\alpha=0$) and Sc>>1.

Since the concentration boundary layer lies well within the hydrodynamic boundary layer, it is useful to rescale the convective-diffusion equation with the hydrodynamic boundary layer thickness. Substituting the stretched variable $\xi = \sqrt{Re}\,\eta$ and the invicid ($Re \rightarrow \infty$) limit of Eq. 26 into Eq. 10 rescales the convective-diffusion equation with respect to the hydrodynamic boundary layer thickness:

$$\frac{1}{Sc}\frac{d^2C}{d\xi^2} + 2\,\varphi(\xi)\frac{dC}{d\xi} = 0 \ , \tag{79}$$

where Sc>>1 and $\varphi(\xi)$ is the classic stagnation point flow solution (see Eq. 27). The boundary conditions for Eq. 79 are $C(0) = 0$ and $C(\infty) = 1$ . Equation 79 describes mass transfer in an axisymmetric stagnation point flow, and asymptotic solutions to this equation are known for Sc>>1 (Chin and Tsang, 1978). The Sherwood number expansion at the substrate disk surface, derived by Chin and Tsang (written here in our variables), is

$$\begin{aligned} Sh = {} & 0.85002\, Re^{1/2} Sc^{1/3} \{1 - 0.084593\, Sc^{-1/3} - 0.016368\, Sc^{-2/3} - \\ & 0.0057398\, Sc^{-1} + 0.0014288\, Sc^{-4/3} + 0.0013088\, Sc^{-5/3} + O(Sc^{-2})\} \ , \end{aligned} \tag{80}$$

when $Re \rightarrow \infty$, $\alpha=0$, and $Sc>>1$. Chin and Tsang have shown that the asymptotic expansion, Eq. 80, is accurate to within one percent of numerical solutions for Schmidt numbers as low as Sc=0.7.

## Discussion

The perturbation expansions given in the Results section were derived by considering limiting values of the dimensionless parameters $\alpha$, Re, Sc, and Pe, or combinations of those parameters. Unfortunately, CVD reactors are rarely operated with extremely large or small Peclet or Reynolds numbers (Patnaik et al., 1989). This means that it is necessary to find the the range of parameters where the Sherwood number expansions are accurate. In this section, we determine the domains of validity for the derived two-term expansions by comparing our analytical expressions for the Sherwood number with numerical results available in the literature.

We begin with the flow field. Recall that $W''(0)$ and $W'''(0)$ are the first two nonzero coefficients in the Taylor series (Eq. 46) and they are functions that can be determined from the asymptotic expansions Eqs. 15a, 21a, and 25. For small Reynolds numbers and $\alpha^2 \leq 1$, $W''(0)$ and $W'''(0)$ are

$$W''(0) = 3 + Re\left(\frac{13}{70} + \frac{\alpha^2}{10}\right) \tag{81}$$

and

$$W'''(0) = -6 - Re\left(\frac{27}{35} + \frac{7\alpha^2}{10}\right). \tag{82}$$

When the Reynolds number is small and $\alpha^2 \geq 1$, $\overline{W}''(0)$ and $\overline{W}'''(0)$ are

$$\overline{W}''(0) = \frac{3}{\alpha} + \overline{Re}\left(\frac{13}{70\alpha^2} + \frac{1}{10}\right) \tag{83}$$

and

$$\overline{W}'''(0) = -\frac{6}{\alpha} - \overline{Re}\left(\frac{27}{35\alpha^2} + \frac{7\alpha^2}{10}\right), \tag{84}$$

and when the Reynolds number is large and $\alpha$=0,

$$W''(0) = -1.13788\,Re^{-1/2} - 1 + 1.317238\,Re^{1/2} \tag{85}$$

and

$$W'''(0) = -Re\ . \tag{86}$$

Recall that Eq. 31 is not valid near the rotating substrate, so evaluating its derivatives at the rotating disk ($\eta$=0) is not appropriate. Shown in Fig. 2 is a comparison between the asymptotic expansions for $W''(0)$ and $W'''(0)$ — Eqs. 81, 82, 85, and 86 — and the numerical results of Wang (1974) as functions of Re when $\alpha = 0$. Figure 2 shows that the low Reynolds number asymptotic expansion holds well even when Re $\approx$ 10. The numerical values of $W''(0)$ and $W'''(0)$ deviate from Eqs. 81 and 82, by 5% and 21%, respectively, when Re=22.5 (and $\alpha$=0). The numerical results also show that the flow field has not yet attained the high Reynolds number asymptotic behavior when Re=53.75 (the largest Re data point shown in Fig. 2). The deviation between the numerical results at Re=53.75 and the asymptotic Eqs. 49 and 50 is about 16% for both expansions. As Re is increased, the accuracy of the large Reynolds number expansions are expected to improve.

Figure 2 does not include the effects of disk rotation. Lance and Rogers (1962) have computed results for rotational flow where one disk is stationary and the other rotates, and there is no injection of fluid (i.e. $\alpha^2 \to \infty$). The calculated values for $\overline{W}''(0)$ showed that small $\overline{Re}$ behavior is maintained when $\overline{Re} \lesssim 15$, and large $\overline{Re}$ asymptotic response is found when $\overline{Re} \gtrsim 250$. This suggests that the low Reynolds number flow near the bottom disk can be estimated by Eq. 81 or Eq. 83 for any $\alpha$ when Re or $\overline{Re}$ is approximately 10 or less.

We next consider the accuracy of the Sherwood number expansions. The Sherwood number is directly proportional to the deposition rate of a mass-transfer-limited species through the relationship

$$v_d = \left(\frac{Dc_i\,\omega_d}{L\,\rho_d}\right) Sh \ , \tag{87}$$

where $v_d$ is the deposition rate of the species, $\omega_d$ is the molecular weight of the deposit species, and $\rho_d$ is the deposit density. Characterizing the parameter space where the Sherwood number expansions are valid is more involved than analyzing the hydrodynamics near the substrate disk, since the Sherwood number response is determined by a greater array of dimensionless parameters.

In Figs. 3 - 6, the Sherwood number is plotted against the Reynolds number for four different values of the Schmidt number and $\alpha$=0. We choose plots of Sh versus Re for constant Sc because one generally has a given set of physical properties that fix Sc, while changing the injection flow rate, the disk gap, or the angular velocity of the disk changes $\alpha$ and Re in the reactor. The reader should keep in mind that the analogy between heat and mass is followed here; for the case of heat transfer, the Prandtl number is analogous the the Schmidt number and the Nusselt number is analogous to the Sherwood number.

We begin the discussion of mass transfer with Figs. 4 and 5, since those figures contain numerical data from Gorla (1984) as well as the perturbation solutions derived in the Results section. Figure 4 shows the dependence of Sh on Re for a typical CVD reactant Schmidt number of Sc=0.7 . Gorla's numerical results fall within 2% of Eq. 41 when Re$\leq$5 and within 0.5% of Eq. 80 for Re$\geq$10 . Equation 41 was derived for Re<<1 and Pe<<1, but we see when $\alpha$=0 and Sc=0.7 the expansion holds even for Re=5 and Pe=3.5 . Similarly, Eq. 80 was derived for Re$\rightarrow\infty$, Pe>>1, and Sc>>1, but Eq. 80 holds even when Re=10, Sc=0.7, and Pe=7. Also plotted in Fig. 4 is Eq. 76, which was derived

for large Re, large Pe, and small Sc. Equation 76 provides a value for Sh that is somewhat larger than Gorla's numerical results when Re>10 and Sc=0.7. The deviation between Eqs. 76 and 80 for high Reynolds numbers is approximately 7% at this Schmidt number. Note also that Eqs. 41 and 80 nearly overlap at Re≈7; the two expansions are within 6% of each other at that Re. Thus, it is possible to obtain the Sherwood number at the substrate to within 6% for any Reynolds number by using simple analytical expressions when Sc=0.7 and $\alpha$=0.

Shown in Fig. 5 is Sh versus Re for a Schmidt number of Sc=10 and $\alpha$=0. Three expansions are plotted along with Gorla's numerical results. It is interesting to note that Eq. 59 serves as an intermediate Sherwood number expansion that overlaps with Eq. 41 to within 0.5% at Re≈0.4 and also overlaps with Eq. 80 to within 5% at Re≈13. Each one of Gorla's numerical data points falls within 3% of an expansion. Therefore, the approximate analytical solutions given by Eqs. 41, 59, and 80, provide estimates for the Sherwood number at the substrate disk that are accurate to within approximately 3% over the entire range of Re, when Sc=10 and $\alpha$=0.

Also included in the series of Sh vs. Re plots are Figs. 3 and 6, for Sc=0.01 and Sc=100, respectively. When the Schmidt number is small (see Fig. 3), Eq. 45 provides an intermediate expansion that overlaps with Eqs. 41 and 76 to within 5%. Similarly, when Sc is large (see Fig. 6), Eq. 59 provides an intermediate expansion that overlaps with Eqs. 41 and 80 to within 5%. The results shown in Figs. 3-6 indicate that an *ad hoc* matching of expansions derived in the Results section provides approximations for the Sherwood number that are accurate to better than ±10% for any combination of Sc, Re, and Pe, when $\alpha$=0. The appropriate intermediate expansion is determined by finding the best overlap of solutions.

Numerical results that show the effects of a rotating disk (i.e. $\alpha \neq 0$) in the self-similar SARDR are limited. Evans and Greif (1988) have recently performed an analysis of self-similar heat transfer in the SARDR system. They show the effects of $\alpha$ on the

Nusselt number for a single Reynolds number (Re=7.842) and Prandtl number (Pr=0.67). Plotted in Fig. 7 (using our variables) are the numerical results of Evans and Greif and Eq. 45 versus $\alpha$, for Sc=0.67. Eq. 45 is used because Re=7.842 falls in the intermediate region where Eqs. 41 and 80 (or Eq. 76) are the least accurate for this Sc, see Fig. 4. Also plotted in Fig. 7 is the expression for the Sherwood number of an infinite rotating disk in an infinite medium as a function of the Reynolds number (Hitchman and Curtis, 1982):

$$\mathrm{Sh} = 0.40\,(\mathrm{Sc}\,\mathrm{Re}\,\alpha)^{1/2}. \tag{88}$$

Hitchman and Curtis report that Eq. 88, which is written here in our variable, is accurate to within 5% of the exact Sherwood number over the range $0.6 \le \mathrm{Sc} \le 6$.

Figure 7 shows that the two-term Sh expansion (Eq. 45) deviates from Evans and Greif's numerical results by less than 5% for $\alpha$ in the range $0 \le \alpha \le 10$. Much of this deviation may come from errors in our linear approximation of $M(\alpha)$, Eq. 30. For large $\alpha$, Sh has a square root dependence on $\alpha$ that follows from Eq. 88, but Evans and Greif's exact numerical values are approximately 7% below the free-disk mass transfer rate.

All of the perturbation expansions derived in the Results section are expected to break down when *either* Pe ~ O(1) or Re ~ O(1). It is rather remarkable that the Sh expansions are accurate to within 10% of the actual values when *both* Pe and Re are O(1), as Figs. 4 and 7 show. In fact, a general trend is observed in Figs. 3 through 7 regarding the crossover point for switching between expansions. Expansions based on high Reynolds number flows (Eqs. 45, 76, and 80) are used when $\mathrm{Re} \ge 12$. When $\mathrm{Re} \le 12$, the low Reynolds number expansions (Eqs. 41 and 59) are used. Moreover, the low Peclet number expansions (Eqs. 41 and 45) are observed to be accurate up to $\mathrm{Pe} \lesssim 5$, provided that the Reynolds number constraints for the fluid mechanics are satisfied. In Fig. 3, for example, Eq. 41 breaks down at $\mathrm{Pe} \approx 0.2$, but that is due to the break down of the low Reynolds number fluid mechanics rather than the break down of the small Peclet number constraint on the expansion. Likewise, the high Pe expansions (Eqs. 59, 76, and 80) appear to hold for $\mathrm{Pe} \ge 5$. The fact that the analytical expansions nearly overlap and are

accurate at intermediate values of Pe and Re indicates that the Sherwood number (and therefore the deposition rate) can be found to better than ±10% for any value of Re, Pe, and Sc in parameter space, at least when $\alpha=0$.

## Implications and Concluding Remarks

We conclude by considering the strengths and shortcomings of applying the model presented here to CVD systems. The design and operation of CVD reactors has been aided significantly by sophisticated numerical studies of the hydrodynamic and transport processes that occur in the reactor. Two-dimensional simulations allow reactor designers to ascertain the desirable operating regimes where deposition is essentially one-dimensional. Unfortunately, much of the fundamental work in CVD transport has required the computational power of advanced supercomputers (Houtman et al., 1986; Evans and Greif, 1987, 1988; Patnaik et al., 1989) and this limits, to a degree, the general availability of such solution techniques. Once the parameter space for one-dimensional, self-similar reactor behavior is known from multidimensional models or experiments, then flexible analytical solutions are useful for providing additional guidelines for the reactor operation. In this paper, we have derived analytical expressions that account for the effects of injection flow rate, the angular velocity of the substrate, and the physical properties of the injected fluid and reactant. Our results compare favorably with numerical simulations.

Several factors that are known to influence the deposition rate and uniformity in CVD have been omitted here. The principal effect neglected is the temperature dependence of physical properties. In CVD, the rotating disk is generally heated to many hundreds of degrees above the temperature of the injected fluid, and this can cause buoyancy driven flows that are undesirable. Deposit uniformity can be maintained in a rotating disk CVD reactor provided that well established constraints on the Grashof and Reynolds numbers are satisfied (Houtman et al., 1986; Evans and Greif, 1987; Patnaik et al., 1989). But axial temperature variations can still modify convective transport in a one-dimensional rotating

disk CVD reactor. Evans and Greif (1988) have shown that the Nusselt number (analogous to Sh) at a heated rotating disk can be less than half the value of a nearly ambient rotating disk in the self-similar SARDR. A less important effect that was neglected is Soret diffusion. An order of magnitude analysis of this phenomena has been given by Patnaik et al. (1989).

We are currently extending the results reported here to consider the two-site adsorption limited kinetics of CdTe organometalic vapor phase epitaxy, the effects of operational parameters on waste reactant discharged from the CVD reactor, and the design of uniform fluid injectors.

## Acknowledgments

This work was supported by the Assistant Secretary for Conservation and Renewable Energy, Office of Energy Storage and Distribution, Energy Storage Division, of the U.S. Department of Energy under Contract No. DE-AC03-76SF00098.

The authors thank R. Greif and G. Evans for providing numerical data, and T.J. Rehg for helpful discussions.

## Notation

$A$ = dimensionless radial pressure coefficient, $-(1/2\lambda)dP/d\lambda$,

$\bar{A}$ = $A/\alpha^2$

$c$ = concentration, mole/m$^3$

$C$ = dimensionless concentration, $c/c_i$

$D$ = mass diffusivity, m$^2$/s

$e_r, e_\theta, e_z$ = unit vectors in cylindrical coordinates

$f$ = radial flow function, s$^{-1}$

$F$ = dimensionless radial flow function, $fL/V$

$\bar{F}$ = $\alpha F$

$g$ = azimuthal flow function, s$^{-1}$

$G$ = dimensionless azimuthal flow function, $g/\Omega$

$\bar{G}$ = $G$

$h$ = mass transfer coefficient, m/s

$L$ = gap thickness between coaxial disks, m

$m$ = stagnation point flow constant, 0.56894

$M(\alpha)$ = far-field rotational constant, $0.56894 - 0.1105\alpha$, when $0 \leq \alpha \leq 10$

$p$ = pressure, kg/m·s

$P$ = dimensionless pressure, $2p/\rho V^2$

$Pe$ = Peclet number, $VL/D$

$\overline{Pe}$ = rotational Peclet number, $\Omega L^2/D$

$R$ = disk radius, m

$Re$ = Reynolds number, $VL/\upsilon$

$\overline{Re}$ = rotational Reynolds number, $\Omega L^2/\upsilon$

$Sc$ = Schmidt number, $\upsilon/D$

$Sh$ = Sherwood number, $hL/D$

$v$ = velocity vector, m/s

$v_d$ = deposition rate, m/s

$V$ = injection velocity, m/s

$w$ = axial velocity, m/s

$W$ = dimensionless axial velocity, $-w/2V$

$\bar{W}$ = $\alpha W$

$z$ = axial distance, m

*Greek letters*

$\alpha$ = inverse Rossby number, $\Omega L/V$

$\varepsilon$ = perturbation parameter

$\Gamma(a)$ = gamma function of a

$\eta$ = dimensionless axial distance, z/L

$\lambda$ = dimensionless radial distance, r/L

$\Omega$ = angular velocity of disk, $s^{-1}$

$\varphi(\xi)$ = dimensionless axial velocity in stagnation point flow

$\Phi$ = axial pressure function

$\rho$ = fluid density, $kg/m^3$

$\rho_d$ = deposit density, $kg/m^3$

$\omega_d$ = molecular weight of deposit species, kg/kg-mole

## Literature Cited

Bird, R.B., W.E. Stewart, and E.N. Lightfoot, *Transport Phenomena*, John Wiley and Sons, New York (1960).

Brady, J.F., and L. Durlofsky, "On Rotating Disk Flow," *J. Fluid Mech.*, **175**, 363 (1987).

Chin, D.-T., and C-H. Tsang, "Mass Transfer to an Impinging Jet Electrode," *J. Electrochem. Soc.*, **125**, 1461 (1978).

Elkouh, A.F., "Laminar Flow Between Rotating Porous Disks," *J. A.S.C.E. Eng. Mech.*, **94**, 919 (1968).

Evans, G., and R. Greif, "A Numerical Model of the Flow and Heat Transfer in a Rotating Disk Chemical Vapor Deposition Reactor," *J. Heat Transfer*, **109**, 928 (1987).

Evans, G.H., and R. Greif, "Forced Flow Near a Heated Rotating Disk: A Similarity Solution," *Numer. Heat Transfer*, **14**, 373 (1988).

Gorla, R.S.R, "Flow and Thermal Characteristics of a Circular Porous Slider Bearing," *Wear*, **94**, 157 (1984).

Hitchman, M.L., and B.J. Curtis, "Heterogeneous Kinetics and Mass Transfer in Chemical Vapor Deposition: III. The Rotating Disc Reactor," *J. Cryst. Growth*, **60**, 43 (1982).

Homann, Von F., "Der Einfluss Grosser Zähigkeit bei der Strömung um den Zylinder und um die Kugel," *Z. Angew. Math. Mech.*, **16**, 153 (1936).

Houtman, C., D.B. Graves, and K.F. Jensen, "CVD in a Stagnation Point Flow," *J. Electrochem. Soc.*, **133**, 961 (1986).

Lance, G.N., and M.H. Rogers, "The Axially Symmetric Flow of a Viscous Fluid Between Two Infinite Rotating Disks," *Proc. Roy. Soc. Lond. A*, **266**, 109 (1962).

Mellor, G.L., P.J. Chapple, and V.K. Stokes, "On the Flow Between a Rotating and a Stationary Disk," *J. Fluid Mech.*, **31**, 95 (1968).

Olander, D.R., "Surface Chemical Kinetics and Gas-Phase Diffusion in the Germanium-Iodine Reaction," *I.&E.C. Fundamentals*, **6**, 178 (1967).

Patnaik, S., R.A. Brown, and C.A. Wang, "Hydrodynamic Dispersion in Rotating-Disk OMVPE Reactors: Numerical Simulation and Experimental Measurements," *J. Cryst. Growth*, **96**, 153 (1989).

Pollard, R., and J. Newman, "Silicon Deposition on a Rotating Disk," *J. Electrochem. Soc.*, **127**, 744 (1980).

Thompson, A.G., V.S. Sundaram, G.R. Girard, and L.M. Fraas, "Growth of GaAs in a Rotating Disk MOCVD Reactor," *J. Cryst. Growth*, 94, 901 (1989).

Tompa, G.S., C.R. Nelson, M.A. Saracino, P.C. Colter, P.L. Anderson, W.H. Wright, and J.L. Schmit, "Multiwafer growth of CdTe on GaAs by Metalorganic Chemical Vapor Deposition in a Vertical, High-Speed, Rotating Disk Reactor," *Appl. Phys. Lett.*, **55**, 62 (1989).

Wang, C.A., S.H. Groves, S.C. Palmateer, D.W. Weyburne, and R.A. Brown, "Flow Visualization Studies for Optimization of OMVPE Reactor Design," *J. Cryst. Growth*, **77**, 136 (1986).

Wang, C.-Y., "Fluid Dynamics of the Circular Porous Slider," *J. Appl. Mechanics*, **41**, 343 (1974).

Wang, C.-Y., "Limitation of the Reynolds Equation for Porous Thrust Bearings," *J. Lubrication Tech.*, **97**, 642 (1975).

Wang, C.-Y., and L.T. Watson, "Viscous Flow Between Rotating Discs with Injection on the Porous Disc," *J. Appl. Math. Phys. (ZAMP)*, **30**, 773 (1979).

Zandbergen, P.J., and D. Dijkstra, "von Kàrmàn Swirling Flows," *Ann. Rev. Fluid Mech.*, **19**, 465 (1987).

## Figure Captions

Fig. 1 Schematic diagram of a small aspect ratio (=L/R) rotating disk CVD reactor. Fluid with dilute reactant is injected at the disk z=L and reaction occurs at the rotating substrate disk z=0.

Fig. 2 Plot of the second and third derivatives of axial velocity evaluated at the substrate disk ($W''(0)$ and $-W'''(0)$) versus Reynolds number for no rotation of the substrate ($\alpha=0$). Comparison between exact numerical results of Wang (1974) and perturbation expansions, Eqs. 81, 82, 85, and 86. Smooth curves are perturbation solutions and data points are numerical solutions. $W''(0)$ is denoted by (——) and (●), and $-W'''(0)$ is denoted by (- - -) and (X).

Fig. 3 Sherwood versus Reynolds number plot for no substrate rotation ($\alpha=0$) and Sc=0.01. Perturbation expansions are given by Eqs. 41 (——), 45 (- - -), and 76 (— — —).

Fig. 4 Sherwood versus Reynolds number plot for no substrate rotation ($\alpha=0$) and Sc=0.7 . Comparison between exact numerical results of Gorla (●) and perturbation expansions, Eqs. 41 (——), 76 (- - -), and 80 (— — —).

Fig. 5 Sherwood versus Reynolds number plot for no substrate rotation ($\alpha=0$) and Sc=10. Comparison between exact numerical results of Gorla (●) and perturbation expansions, Eqs. 41 (——), 59 (- - -), and 80 (— — —).

Fig. 6 Sherwood versus Reynolds number plot for no substrate rotation ($\alpha$=0) and Sc=100. Perturbation expansions are given by Eqs. 41 (——), 59 (- - -), and 80 (— — —).

Fig. 7 Substrate rotation effect. Sherwood versus inverse Rossby number plot for Sc=0.67 and Re=7.842. Comparison between exact numerical results of Evans and Greif (1988) (●), perturbation expansion, Eq. 45 (——), and solution for a rotating disk in an infinite medium, Eq. 88 (— — —).

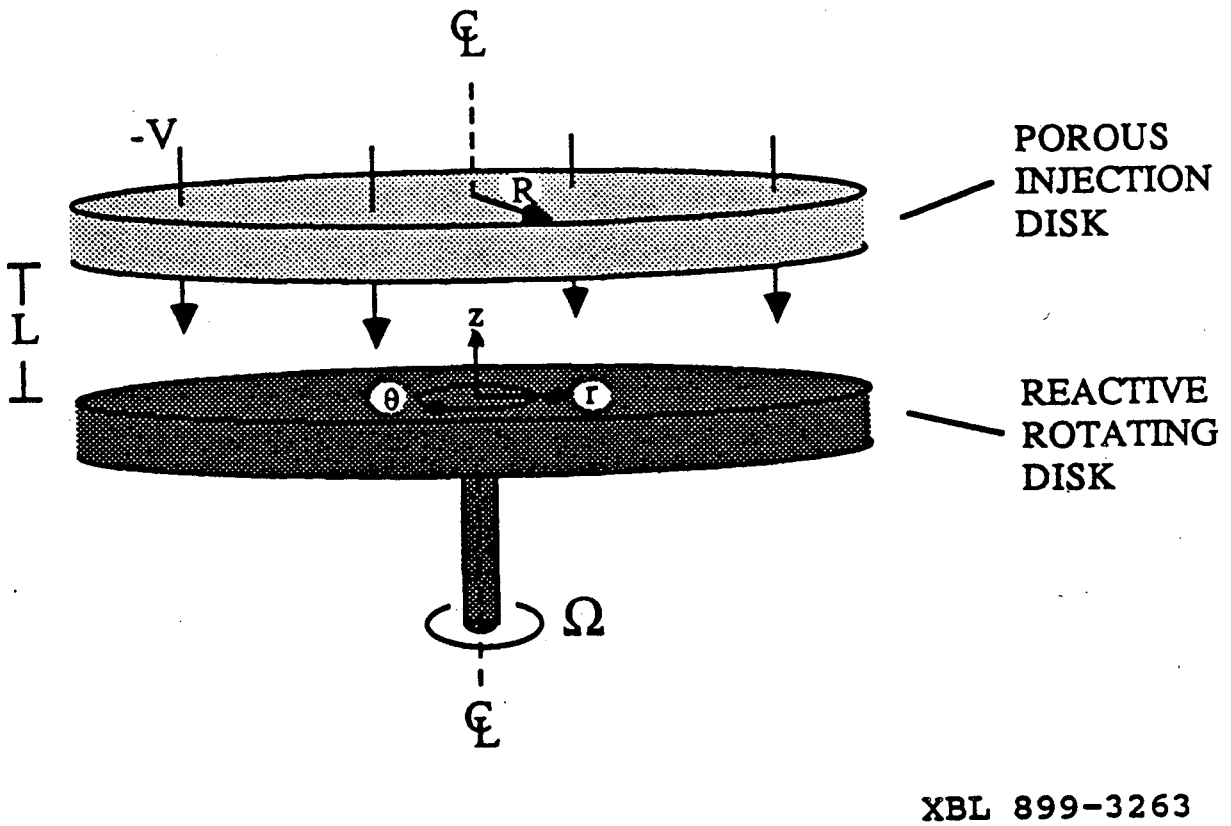


Fig. 1 Schematic diagram of a small aspect ratio (=L/R) rotating disk CVD reactor. Fluid with dilute reactant is injected at the disk z=L and reaction occurs at the rotating substrate disk z=0.

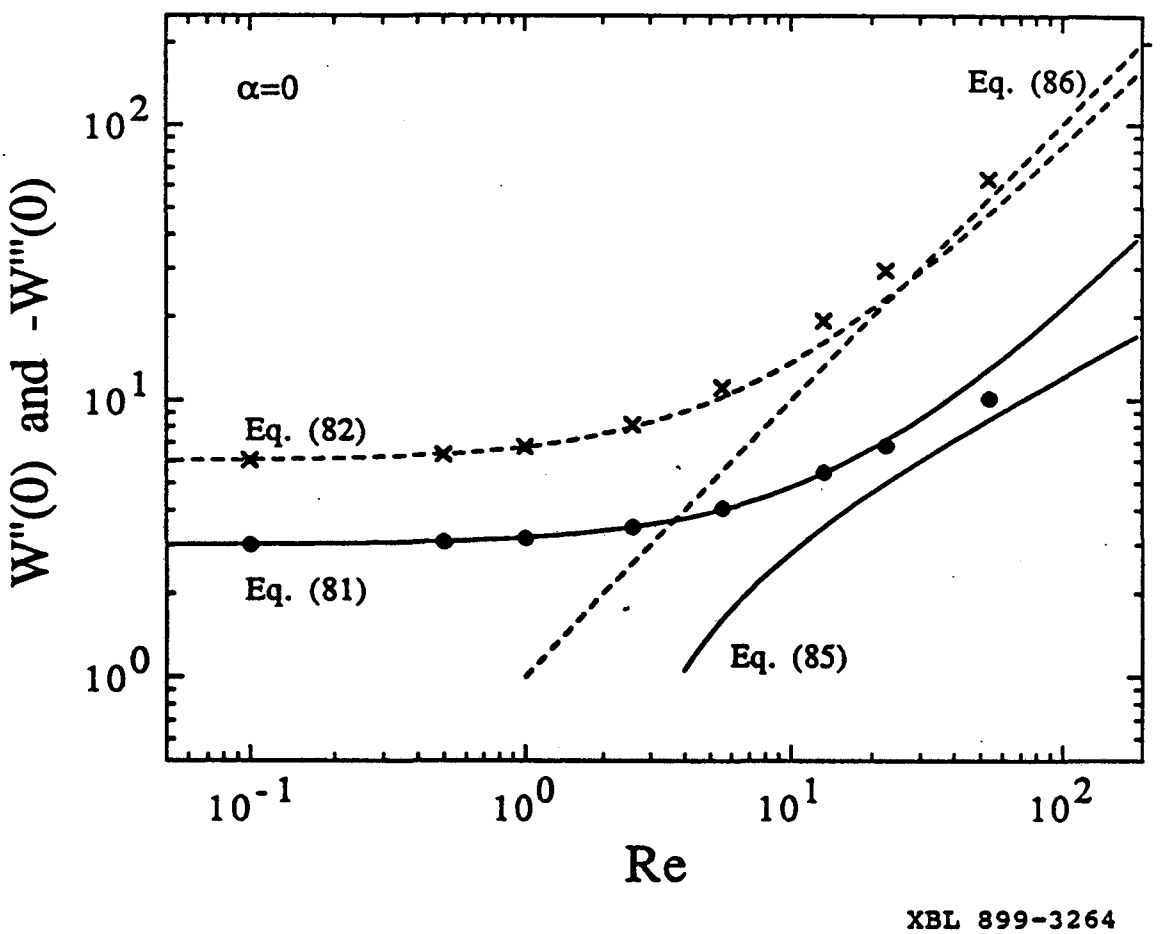


Fig. 2 Plot of the second and third derivatives of axial velocity evaluated at the substrate disk (W''(0) and -W'''(0)) versus Reynolds number for no rotation of the substrate (α=0). Comparison between exact numerical results of Wang (1974) and perturbation expansions, Eqs. 81, 82, 85, and 86. Smooth curves are perturbation solutions and data points are numerical solutions. W''(0) is denoted by (——) and (●), and -W'''(0) is denoted by (- - -) and (X).

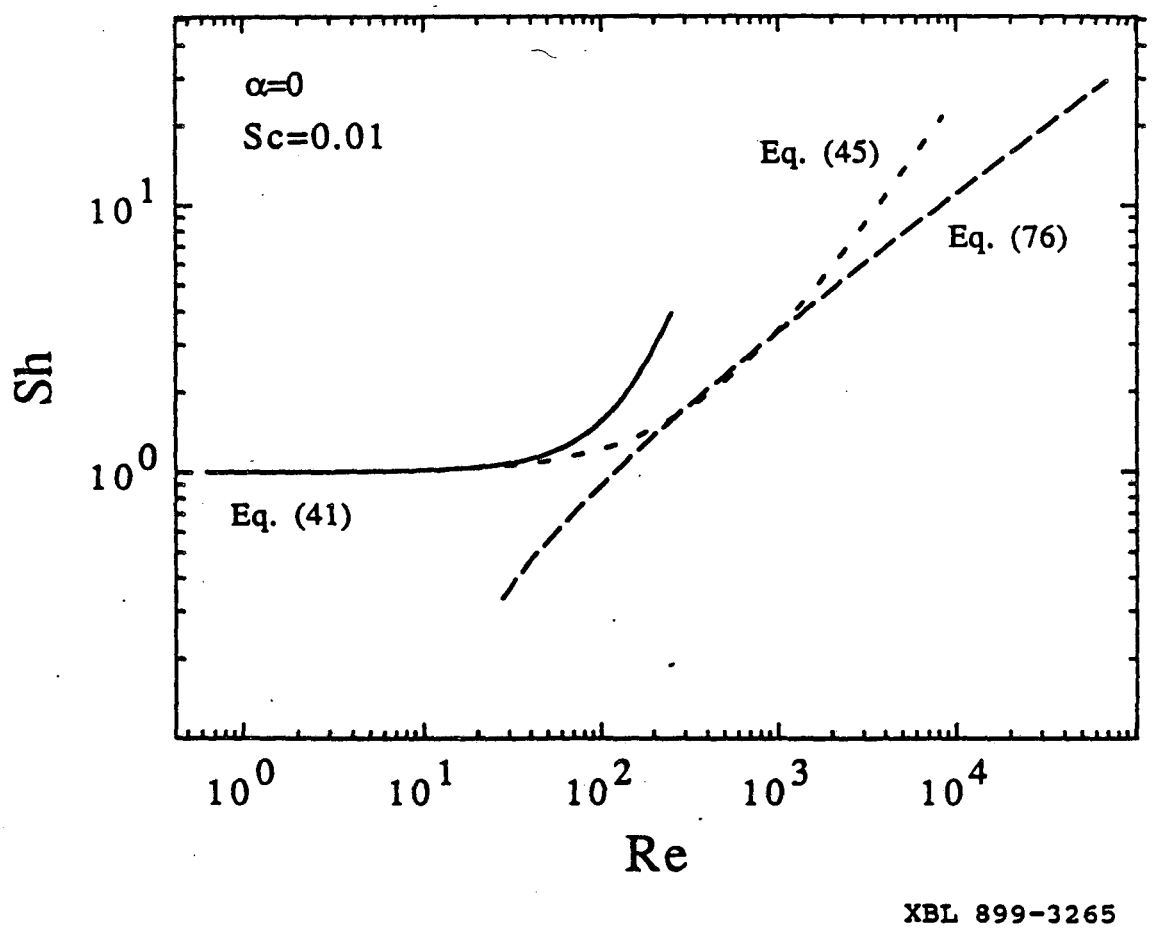


Fig. 3 Sherwood versus Reynolds number plot for no substrate rotation (α=0) and Sc=0.01. Perturbation expansions are given by Eqs. 41 (——), 45 (- - -), and 76 (— — —).

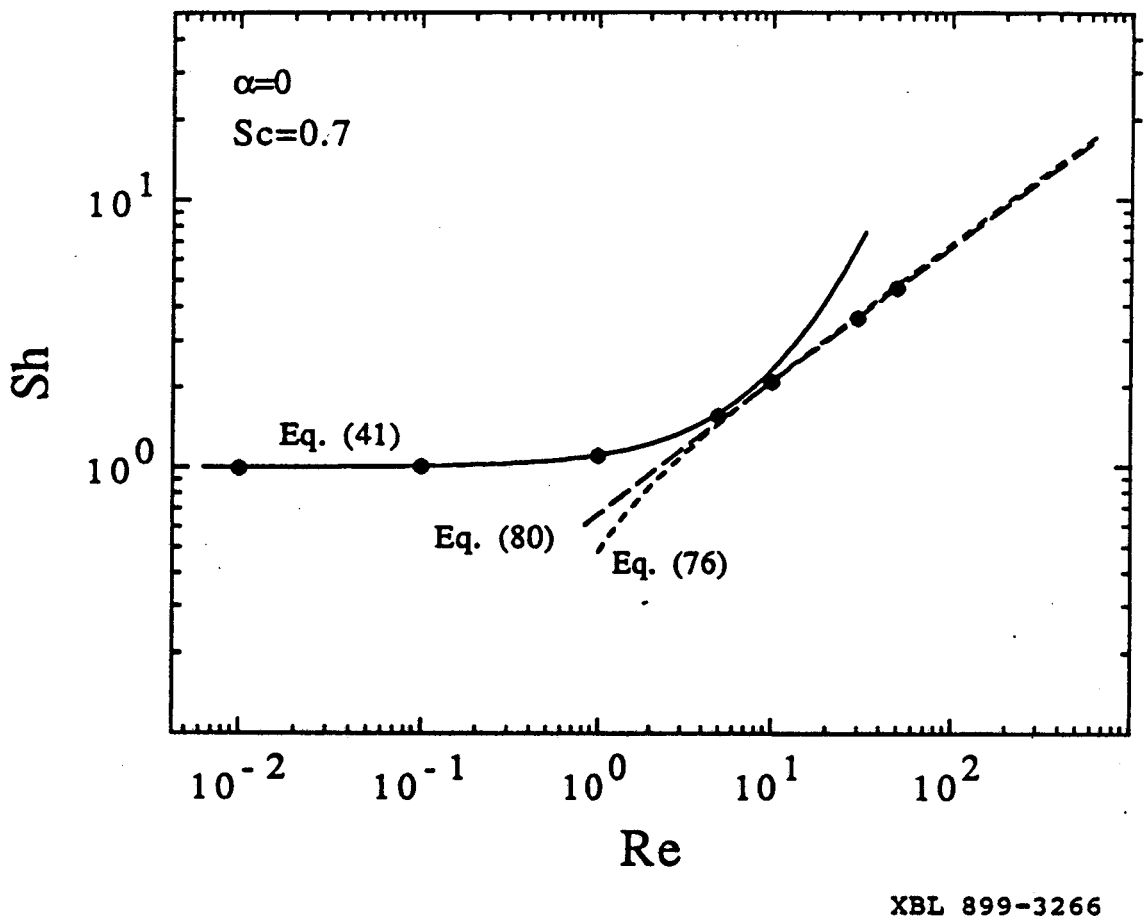


Fig. 4 Sherwood versus Reynolds number plot for no substrate rotation ($\alpha$=0) and Sc=0.7 . Comparison between exact numerical results of Gorla (●) and perturbation expansions, Eqs. 41 (——), 76 (- - -), and 80 (— — —).

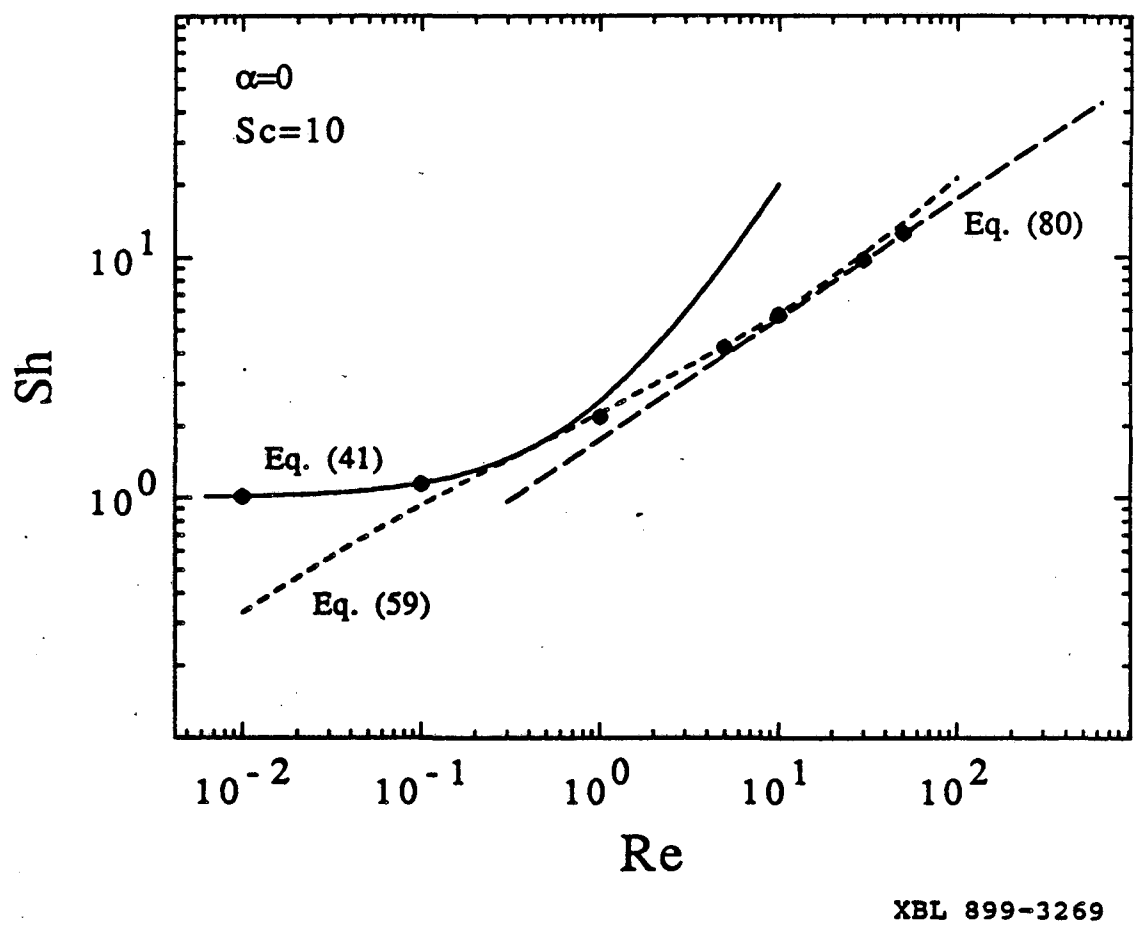


Fig. 5 Sherwood versus Reynolds number plot for no substrate rotation (α=0) and Sc=10. Comparison between exact numerical results of Gorla (●) and perturbation expansions, Eqs. 41 (——), 59 (- - -), and 80 (— — —).

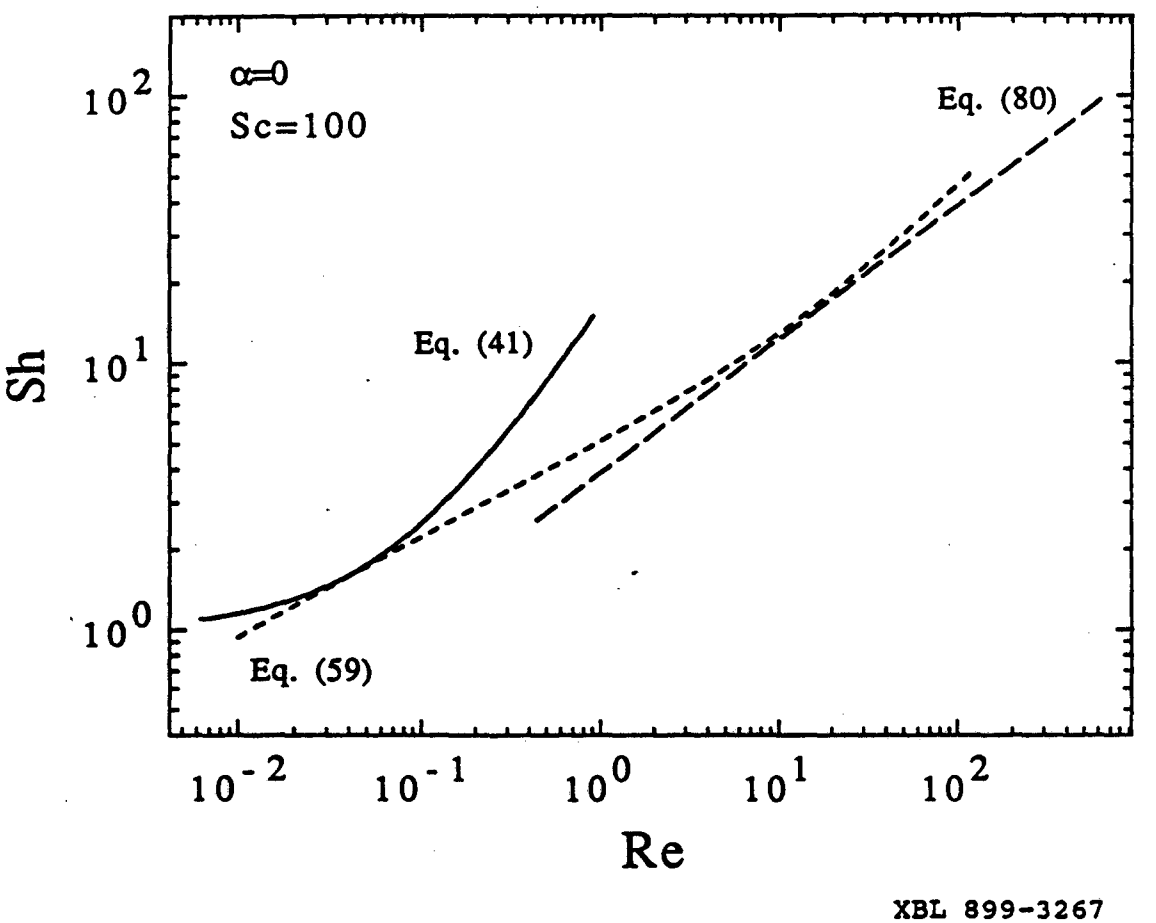


Fig. 6 Sherwood versus Reynolds number plot for no substrate rotation ($\alpha$=0) and Sc=100. Perturbation expansions are given by Eqs. 41 (——), 59 (- - -), and 80 (— — —).

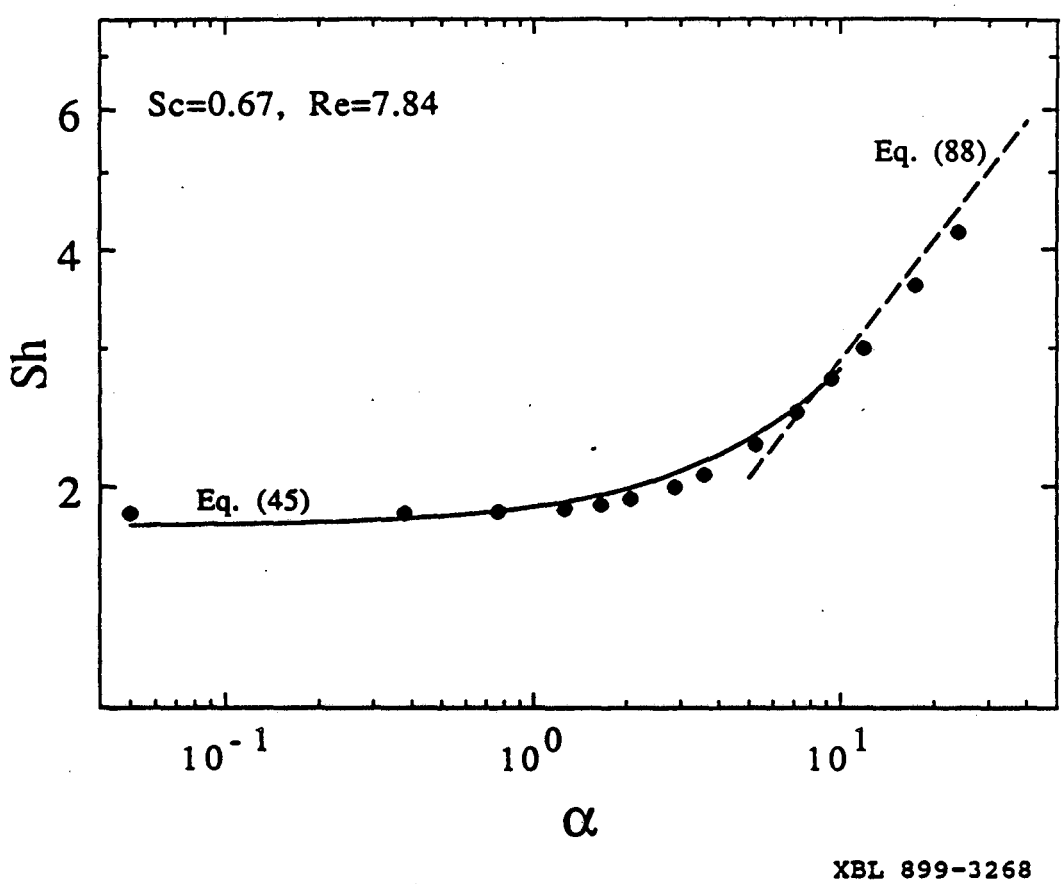


Fig. 7 Substrate rotation effect. Sherwood versus inverse Rossby number plot for Sc=0.67 and Re=7.842. Comparison between exact numerical results of Evans and Greif (1988) (●), perturbation expansion, Eq. 45 (——), and solution for a rotating disk in an infinite medium, Eq. 88 (— — —).

LAWRENCE BERKELEY LABORATORY
TECHNICAL INFORMATION DEPARTMENT
1 CYCLOTRON ROAD
BERKELEY, CALIFORNIA 94720